remote sensing

MDPI

Article

Synergistic Potential of Optical and Radar Remote Sensing for Snow Cover Monitoring

Jose-David Hidalgo-Hidalgo [1], Antonio-Juan Collados-Lara [2,3], David Pulido-Velazquez [1], Steven R. Fassnacht [1,4,5,*] and C. Husillos [6]

[1] Spanish Geological Survey, Water and Global Change Research, 18006 Granada, Spain; jd.hidalgo@igme.es (J.-D.H.-H.); d.pulido@igme.es (D.P.-V.)
[2] Department of Civil Engineering, University of Granada, 18071 Granada, Spain; ajcollados@ugr.es
[3] Department of Geology, University of Jaén, 23071 Jaén, Spain; ajcl0021@ext.ujaen.es
[4] ESS-Watershed Science, Colorado State University, Fort Collins, CO 80523-1476, USA
[5] Cooperative Institute for Research in the Atmosphere, Fort Collins, CO 80523-1375, USA
[6] Spanish Geological Survey, Unit of Development and Dissemination of Information Systems, 18006 Granada, Spain; c.husillos@igme.es
* Correspondence: steven.fassnacht@colostate.edu; Tel.: +1-970-491-5454

Abstract: This research studies the characteristics of snow-covered area (SCA) from two vastly different sensors: optical (Moderate-Resolution Imaging Spectroradiometer, or MODIS, equipped on board the Terra satellite) and radar (Synthetic Aperture Radar (SAR) on-board Sentinel-1 satellites). The focus are the five mountain ranges of the Iberian Peninsula (Cantabrian System, Central System, Iberian Range, Pyrenees, and Sierra Nevada). The MODIS product was selected to identify SCA dynamics in these ranges using the Probability of Snow Cover Presence Index (PSCPI). In addition, we evaluate the potential advantage of the use of SAR remote sensing to complete optical SCA under cloudy conditions. For this purpose, we utilize the Copernicus High-Resolution Snow and Ice SAR Wet Snow (HRS&I SWS) product. The Pyrenees and the Sierra Nevada showed longer-lasting SCA duration and a higher PSCPI throughout the average year. Moreover, we demonstrate that the latitude gradient has a significant influence on the snowline elevation in the Iberian mountains ($R^2 \geq 0.84$). In the Iberian mountains, a general negative SCA trend is observed due to the recent climate change impacts, with a particularly pronounced decline in the winter months (December and January). Finally, in the Pyrenees, we found that wet snow detection has high potential for the spatial gap-filling of MODIS SCA in spring, contributing above 27% to the total SCA. Notably, the additional SCA provided in winter is also significant. Based on the results obtained in the Pyrenees, we can conclude that implementing techniques that combine SAR and optical satellite sensors for SCA detection may provide valuable additional SCA data for the other Iberian mountains, in which the radar product is not available.

Keywords: snow-covered area; SAR; optical and radar; satellite; wet snow; snow; remote sensing; Iberian Peninsula

Citation: Hidalgo-Hidalgo, J.-D.; Collados-Lara, A.-J.; Pulido-Velazquez, D.; Fassnacht, S.R.; Husillos, C. Synergistic Potential of Optical and Radar Remote Sensing for Snow Cover Monitoring. *Remote Sens.* **2024**, *16*, 3705. https://doi.org/10.3390/rs16193705

Academic Editors: Mircea Alexe, Iulian-Horia Holobâcă and Noel Aloysius

Received: 2 August 2024
Revised: 24 September 2024
Accepted: 26 September 2024
Published: 5 October 2024

1. Introduction

Snow cover is fundamental to the Earth's energy balance and moisture fluxes between the surface and the atmosphere, playing a crucial role in regulating the global climate [1]. Snow is also an essential component of both natural and human systems, exerting significant influence on water resources [2], agriculture [3,4], ecology [5–7], socioeconomics [8–10], tourism [11–13], and hydropower generation [14,15]. The critical importance of snow and the snow-covered area (SCA) in numerous system processes on Earth has prioritized the development of techniques for measuring SCA dynamics. These techniques include in situ sensors, hydrological modeling, and, most prominently, remote sensing [16–18]. Ground-based observations of SCA in alpine regions are relatively recent and sparsely distributed

due to the adverse conditions that complicate data collection. Likewise, despite great advances in SCA modeling in recent years [19–21], there remains a need for deeper physical understanding and proper calibration [22,23].

Remote sensing programs have significantly increased the number of available data sources for SCA monitoring, enhancing our ability to track and analyze SCA dynamics on a broader scale [24,25]. In particular, optical satellite sensors have been extensively used for snow observation worldwide [26,27]. Among these sensors, the Moderate-Resolution Imaging Spectroradiometer (MODIS) holds a prominent position in hydrological studies due to its sufficiently high spatial resolution for global scale SCA monitoring, high temporal resolution, and relatively long data records [28–30]. SCA detection with MODIS achieves good overall accuracy for SCA detection (around 93%) [31], although its effectiveness can diminish in densely forested areas (around 71% in areas exceeding 50% of tree cover density) where the canopy obscures the underlying snowpack [32]. However, cloud cover conditions and dark night remain the main limitations of optical remote sensing, as they prevent the capture of reflectivity of the Earth's surface [33–35]. Consequently, prolonged periods cannot be observed with optical sensors, particularly in frequently clouded areas or regions with limited sunlight.

An alternative to optical sensors for SCA monitoring is microwave remote sensing [36–38], which enables snow observation independently of weather and solar illumination conditions. Active microwave sensors, specifically Synthetic Aperture Radar (SAR), are the most commonly used for global-scale snow monitoring due to their high spatial resolution compared to passive microwave sensors [39]. The most widely used method for snow monitoring with SAR remote sensing is the backscattering-based method, commonly called Nagler's method [40,41]. However, unlike optical remote sensing, the backscattering-based method is sensitive to snow state (dry or wet). Snow is a mixture of ice crystals, liquid water, and air. Dry snow is below 0 °C and, thus, only composed of ice particles and air. On the contrary, wet snow is at temperatures at or above 0 °C, so that its composition also includes significant quantities of liquid water [42]. At C- and X-band low microwave frequencies (4 to 8 GHz and 8 to 12 GHz, respectively), SAR remote sensing has demonstrated high potential for wet snow mapping [43]. At these frequencies, an increase in the liquid water content within the snowpack significantly reduces the radar backscattering signal in relation to snow-free and dry snow surfaces [44,45]. In recent years, the European Space Agency's Copernicus program launched the Sentinel-1 mission, which is equipped with C-band SAR for land monitoring [46]. To leverage the capabilities of the Sentinel-1 constellation in cryosphere studies, the Copernicus Land Monitoring Service recently developed the High-Resolution Snow and Ice (HRS&I) project for wet snow monitoring in mountainous regions by means of the use of the backscattering-based method [40,41].

In this article, we aim to characterize the SCA dynamics in the main snow-dominated mountain ranges of the Iberian Peninsula. Firstly, we contrast the differences in SCA (Probability of Snow Cover Presence Index, hereinafter PSCPI, and snow season length) across these montane regions based on specific elevation ranges and latitude. Secondly, we appraise the correlation between geographical location (latitude) and spatial meteorological variables (temperature and precipitation) with SCA characteristics. In this study, as a novel aspect, we also aim to evaluate the potential contribution of radar remote sensing data from SAR in characterizing the SCA dynamics of the main snow-dominated mountain ranges in the Iberian Peninsula. The SAR product for spatial gap-filling optical remote sensing for snow cover monitoring is currently available only for the Pyrenees in the Iberian Peninsula. In this article, we aim to demonstrate the utility of this product for the other snow-dominated mountain ranges in the Iberian Peninsula, including Europe's southernmost mountain. We considered MODIS as the base for the computation of the PSCPI, which illustrates the differences in SCA dynamics among the mountain ranges. Furthermore, we utilized the AEMET 5 km climate dataset to relate SCA dynamics with precipitation and temperature patterns. Finally, we used the HRS&I SWS product to evaluate the additional SCA that radar remote sensing can provide for filling spatial gaps

in optical satellite sensors (MODIS) under cloud cover conditions. This analysis involved comparing and combining both products (HRS&I SWS and MODIS) on the same dates in the Pyrenees (the only Iberian montane region available in the HRS&I SWS product).

2. Study Sites

The Iberian Peninsula features highly irregular orography characterized by extensive mountainous massifs spread across its main snow-dominated mountain ranges (Cantabrian System, Central System, Iberian Range, Pyrenees, and Sierra Nevada) (Figure 1). Positioned between the Atlantic Ocean and the Mediterranean Sea, together with its intricate topography, the Iberian Peninsula experiences a diverse climatic regime. Precipitation exhibits a notable negative gradient from the northwest to the southeast, with the northwestern quadrant receiving an annual average precipitation exceeding 1000 mm [47], mainly influenced by the North Atlantic Oscillation and the Arctic Oscillation [48]. In contrast, the southeastern quadrant is dominated by the Western Mediterranean Oscillation with annual average precipitation records below 300 mm. On the other hand, temperature displays a discernible positive gradient from north to south and from coastal areas towards inland regions [49]. Winter temperatures are frequently colder than 0 °C in the main mountain ranges, depending on elevation. The substantial climatic variations, along with differences in latitude, elevation, and proximity to the coast among the main mountain ranges of the Iberian Peninsula, significantly influence SCA distribution, snow season length, and the dynamics of the melting–freezing processes during the snow season.

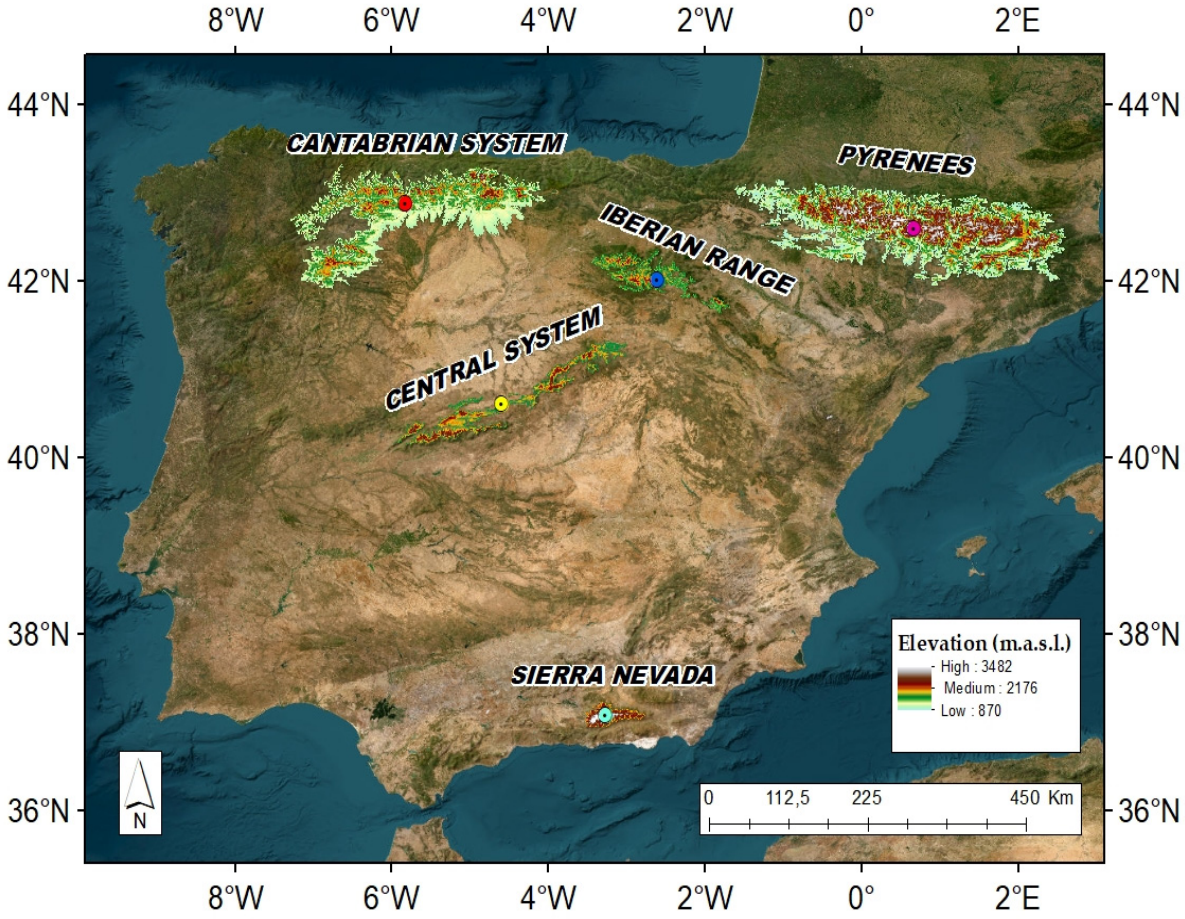

Figure 1. Location of the main snow-dominated mountain ranges of the Iberian Peninsula. The circle points indicate the centroid of each mountain range.

3. Data and Methods

3.1. Methods

In this research, we propose a methodology for the analysis of SCA characteristics in the main snow-dominated montane regions of the Iberian Peninsula. Furthermore, we assess the potential advantage of the combination of SAR and optical remote sensing for SCA monitoring in the Iberian mountains (Figure 2). The proposed methodology includes the following steps: (1) SCA characterization in terms of PSCPI and snow season length, as well as the determination of the degree of relationship between the latitude and snowline elevation in the Iberian mountains; (2); the assessment of the recent climate change impacts on snow cover (3); the analysis of the potential of SAR for spatial gap-filling optical remote sensing SCA data; and (4) the evaluation of the potential limitations of optical and SAR remote sensing for SCA monitoring.

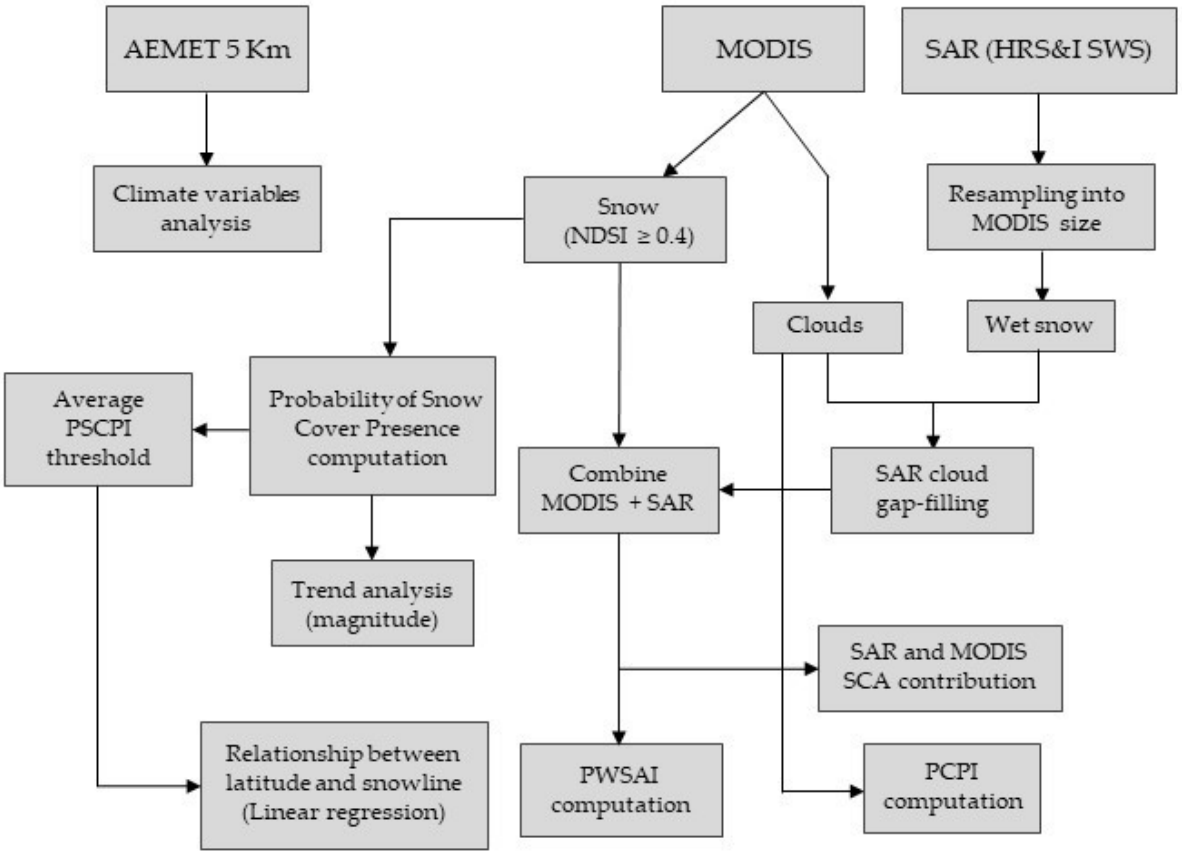

Figure 2. Flowchart of the methodology.

3.1.1. Snow Characteristics

The focus montane regions are distributed throughout the Spanish territory, necessitating the merging of data from multiple MODIS granules (h17v04, h17v05, and h18v04) using the HDF-EOS to GeoTIFF Conversion Tool. For the comparison among the different mountain ranges, we used the Probability of Snow Cover Presence Index (PSCPI) [50], which is computed pixel-by-pixel as follows:

$$PSCPI = \frac{N_S}{N_A} \times 100 \quad (1)$$

where N_S is the number of days with snow cover presence (days where the NDSI equals or exceeds the standard threshold of 0.4) and N_A is the number of days with available NDSI data, so that it refers to the average number of days covered by snow over the 23-year period of records. In this study, snow cover on a pixel was defined when the NDSI is

equal or exceeds the standard NDSI threshold of 0.4 [51]. This threshold has traditionally been used and corresponds to a fractional snow cover equal to or exceeding 50% [52,53]. Recent research suggests that this threshold value may not be optimal for local-scale studies [54]; however, it has been demonstrated to be suitable for products with moderate spatial resolution (around 500 m or greater) for SCA classification [54,55]. Subsequently, we determined the average PSCPI at 10 m elevation intervals and then defined the area of interest of each mountain range as the regions where the average PSCPI exceeds 1.5%. To establish the elevation interval, it was essential to ensure an adequate number of MODIS cells for calculating the average PSCPI in the smallest mountain range within the Iberian Peninsula. It is important to note that the Iberian mountains vary considerably in size, with larger mountains providing a greater number of MODIS cells for calculating the average PSCPI. These defined domains were utilized to analyze various snow-related questions proposed in this study, providing insights into SCA dynamics across different elevations within each mountain range.

Firstly, we realized an intercomparison of PSCPI variations with elevation among the mountain ranges of the Iberian Peninsula. Secondly, we compared the duration of the snow-covered season delineated across diverse elevation intervals defined at 500 m increments with the aim of discerning potential differences among mountain ranges and within specific elevation bands. Snow season duration is defined as the time interval with consistency on snow cover, which is determined by onset and offset dates. In this research, the onset of the snow season was identified as the first day when the PSCPI surpasses 10% and remains at or above this value for at least two-thirds of the time over the following four weeks. The offset of the snow season was qualitatively defined as the first day when the PSPI reaches minimum values and remains at those levels for at least two consecutive weeks. Furthermore, we examined the relationship between latitude and the elevation of the snowline. This analysis involved determining snowline elevations under various PSCPI thresholds. The strength of the relationship between the latitude and elevation of the snowline was assessed using the coefficient of determination (R^2) from a linear regression.

3.1.2. Analysis of the Recent Impacts of Climate Change on Snow Cover

To assess the temporal changes in SCA, we set the time span at a 5-year period (lustrum) due to the relatively short time coverage of MODIS records. This allowed us to determine the magnitude of the trend (slope), based on the average PSCPI, across the entire domain of each mountain range for four lustra (2001–2005, 2006–2010, 2011–2015, and 2016–2020) at a monthly scale. As suggested in previous studies, summer SCA time series may not be suitable for trend analysis [56], so we restricted our analysis to the snow season months (November to May).

In this study, both parametric and non-parametric methods were employed to detect the magnitude of SCA trend. A linear regression analysis was used to estimate the trend's rate when the SCA time series were normally distributed; otherwise, we performed a non-parametric Sen's slope estimator [57]. Rates are shown as% per lustrum (%/lustrum). To assess normality, we decided on the Anderson–Darling test [58,59] with a significance level of 5%. When $p < 0.05$, the null hypothesis is rejected, indicating that the SCA time series does not follow a normal distribution.

3.1.3. Assessment of the Synergistic Use of SAR and Optical Remote Sensing

The potential use of the HRS&I SWS product to complement the SCA provided by MODIS in the Iberian mountains was evaluated, specifically focusing on assessing the additional SCA data from HRS&I SWS compared to MODIS in the Pyrenees. It is noteworthy that the HRS&I SWS product is available exclusively for this montane region within the Iberian Peninsula. This evaluation was conducted monthly throughout the snow season (November to May). Firstly, we aligned and rescaled the HRS&I SWS product to match the MODIS granule alignment and pixel size, ensuring accurate comparison between

the two datasets. Subsequently, we developed an index called Probability of Wet Snow Additional Information (PWSAI), calculated as follows:

$$PWSAI = \frac{N_W}{N_T} \times 100 \quad (2)$$

where N_W is the number of days with at least one additional pixel with wet snow (HRS&I SWS) under cloudy conditions in the MODIS product, and N_T is the number of days with data available about snow cover in both products (HRS&I SWS and MODIS) on the same date. Secondly, we analyzed the respective contributions of each product to the total SCA. It is important to note that we only considered wet snow data under cloud cover conditions and ensured a correct comparison between the two products exclusively contrasting data from the same date (MODIS and HRS&I products have different temporal resolutions). Moreover, we evaluated the range of variability of the wet snow contribution to the total SCA for each month.

3.1.4. Potential Sources of Distortion of SAR and Optical Remote Sensing

Snow cover classification with optical and SAR remote sensing methods can be affected by various factors such as cloud coverage (only relevant for optical sensors) and dense forest canopy, among others (for more detailed information, see Appendix A). To address these challenges, we assessed the probability of cloud cover presence (from here on: PCPI) pixel-by-pixel on a monthly basis within each mountain range, applying a similar procedure to the one used for the calculation of the PSCPI. The PCPI is defined as the ratio of days with cloud cover to days with available data (non-filled data), representing the average occurrence of cloudy conditions over the 23-year period of records. Additionally, we evaluated the average probability of forest density at 10 m elevation intervals within each mountain range.

3.2. Data

3.2.1. Climatological Data

The AEMET 5 km dataset [60,61], obtained from the Spanish Meteorological Agency, was chosen for this study because it offers extensive temporal coverage with suitable temporal resolution (daily) and a spatial resolution of 5 km of the climatic variables (precipitation and temperature). This long-term series can be useful to perform analyses of drought propagation and their statistics [62–64].

Due to the coarse spatial resolution of this dataset, a distributed analysis of the climatic variables was not feasible; therefore, we conducted a lumped one. Precipitation analysis was performed for the entire domain of the mountain ranges, while temperature analysis was conducted within the common elevation range for the Iberian mountains (1600–2300 m.a.s.l.) to facilitate proper comparison, considering the strong elevation influence on temperature at both regional [65] and local scales [66,67]. Precipitation and temperature series were aggregated using a weighted average, conducted by the Thiessen polygon method [68]. In this method, each point within the considered elevation range was assigned a weight based on its relative area in relation to the total area.

3.2.2. Snow Data

The optical snow cover satellite dataset selected for this study was the MODIS Terra Snow Cover Collection 6 product [69]. This dataset offers long-term insights into the Normalized Difference Snow Index (NDSI), represented as a percentage ranging from 0 to 100%, alongside binary delineations for various screened-out areas such as cloud cover. It offers moderate spatial resolution (500 m) and a high temporal resolution (daily). The NDSI is a dimensionless index that ranges from −1 to 1, but, in this dataset, negative NDSI values have been set to 0 (for a more detailed description of this index, see Appendix A). In this research, we used snow cover records spanning the period from 1 March 2000 until 31 May 2023.

The Copernicus HRS&I SWS product provides information about wet snow and various features prone to interference with the radar backscattering signal, such as shadow, layover or foreshortening, forest areas, urban infrastructures, and water bodies. This dataset is available for specific mountainous regions of the European continent (the Alps, Eastern Turkey, Iceland, the Pyrenees, and Scandinavia) with a high spatial resolution of 60 m every 6 days. In this research, we focused on the Pyrenees (the only mountain range available in the Iberian Peninsula) and utilized the HRS&I SWS data from both ascending and descending orbits for the period from 1 November 2016 to 31 May 2023.

3.2.3. Forest Density Data

The High-Resolution Layer Tree Cover Density dataset furnishes insights into tree cover density (TCD, represented as a percentage ranging from 0% to 100%), which is defined as the vertical projection of tree crowns to the horizontal surface of the Earth. This product is provided for the reference year 2018 at a pan-European level (EEEA38 countries and United Kingdom) with a high spatial resolution of 10 m.

4. Results

An analysis of temperature trends across the Iberian mountains revealed the Pyrenees as the coldest range during winter (considered as the time span from December to February), approximately 2 °C cooler than the Cantabrian and Iberian Ranges, and 3.5 °C cooler than the Central System and the Sierra Nevada. In spring (considered as the time interval from March to May), despite temperatures in the mid-spring period becoming similar to the Cantabrian System, the Pyrenees initially showed a colder trend. Conversely, the warmest temperatures were observed in the Sierra Nevada during winter and the Central System during spring (Figure 3b). Additionally, precipitation patterns across different mountain ranges were contrasted, highlighting the Cantabrian System and the Pyrenees as receiving the highest average accumulated precipitation during winter (506 mm) and spring (323 mm), respectively. In contrast, the Sierra Nevada exhibited the lowest precipitation levels in both winter (332 mm) and spring (132 mm) (Figure 3a).

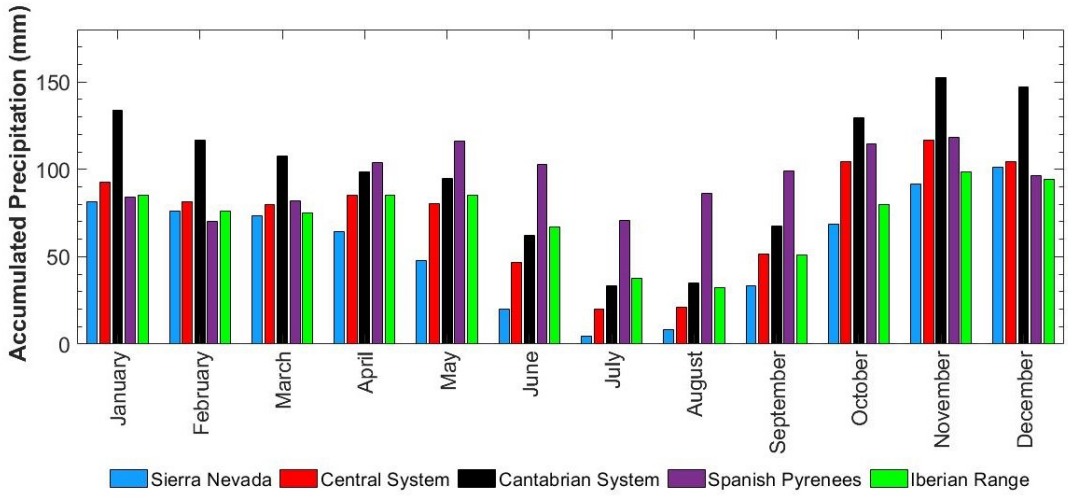

(**a**)

Figure 3. *Cont.*

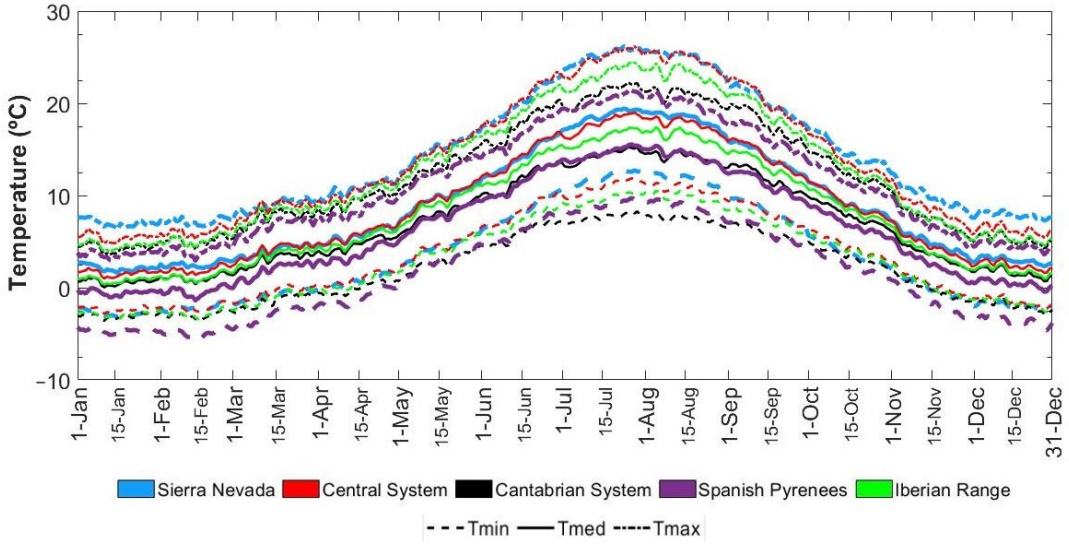

(**b**)

Figure 3. Aggregated climate variables sourced from the AEMET 5 km dataset to appraise the differences between Iberian montane regions over an average year for (**a**) mean monthly accumulated precipitation and (**b**) minimum, average, and maximum temperature.

4.1. Evaluation of Snow Characteristics

The major factors influencing the PSCPI in the main snow-dominated mountains of the Iberian Peninsula are latitude and elevation. The influence of elevation becomes noticeable when comparing ranges within the same elevation band. For instance, the Sierra Nevada and the Pyrenees (the highest mountain ranges of the Iberian Peninsula), both reaching elevations above 2500 m.a.s.l. (up to 3400 m.a.s.l.), exhibit maximum PSCPI values close to 80% (Figure 4a,b). In contrast, the Cantabrian System, Central System, and Iberian Range show significantly lower values: 44%, 32%, and 27%, respectively. An intercomparison of mountain ranges within particular elevation ranges evidences that latitude predominantly influences the PSCPI across the Iberian mountains. Generally, higher average PSCPI values are observed in mountain systems located at higher latitudes, except for the Central System at elevations around 2500 m.a.s.l. where the average PSCPI is slightly lower than that of the Sierra Nevada (23% vs. 27%) (Figure 4a,e). Moreover, despite the higher latitude of the Iberian Range, it shows similar average PSCPI values above 2000 m.a.s.l. compared to the Central System (around 20%) (Figure 4d).

The daily distribution of the PSCPI varies across different mountain ranges and within each mountain range according to elevation bands (Figure 5). A long-lasting snowpack exists in all Iberian mountains above 2000 m.a.s.l. A comparison at the common 2000–2500 m.a.s.l. elevation band underlines a longer snowpack duration in the mountain ranges located at higher latitudes (237 days in the Pyrenees and 229 days in the Cantabrian System), whereas snowpack durations are notably shorter in the other ranges (184 days in the Iberian Range, 182 days in the Central System, and 175 days in the Sierra Nevada). Nonetheless, at elevations above 2500 m.a.s.l. (only the Pyrenees and the Sierra Nevada), differences on snowpack persistence related to latitude are markedly reduced since the snow season length above this elevation is relatively similar (275 days vs. 244 days) (Figure 5). In the summer months, we observe that a continuous and confined snowpack persists above 2500 m.a.s.l. in the Pyrenees (PSCPI around 5%). In the Iberian mountains, snowmelt begins primarily in late March; however, this timing is strongly dependent on elevation. Snowmelt occurs progressively later as elevation increases within each mountain range. Consequently, at higher elevation in the Sierra Nevada and the Pyrenees (the highest mountain ranges), snowmelt not only starts later but also progresses at a faster rate compared to the other ranges (Figure 5).

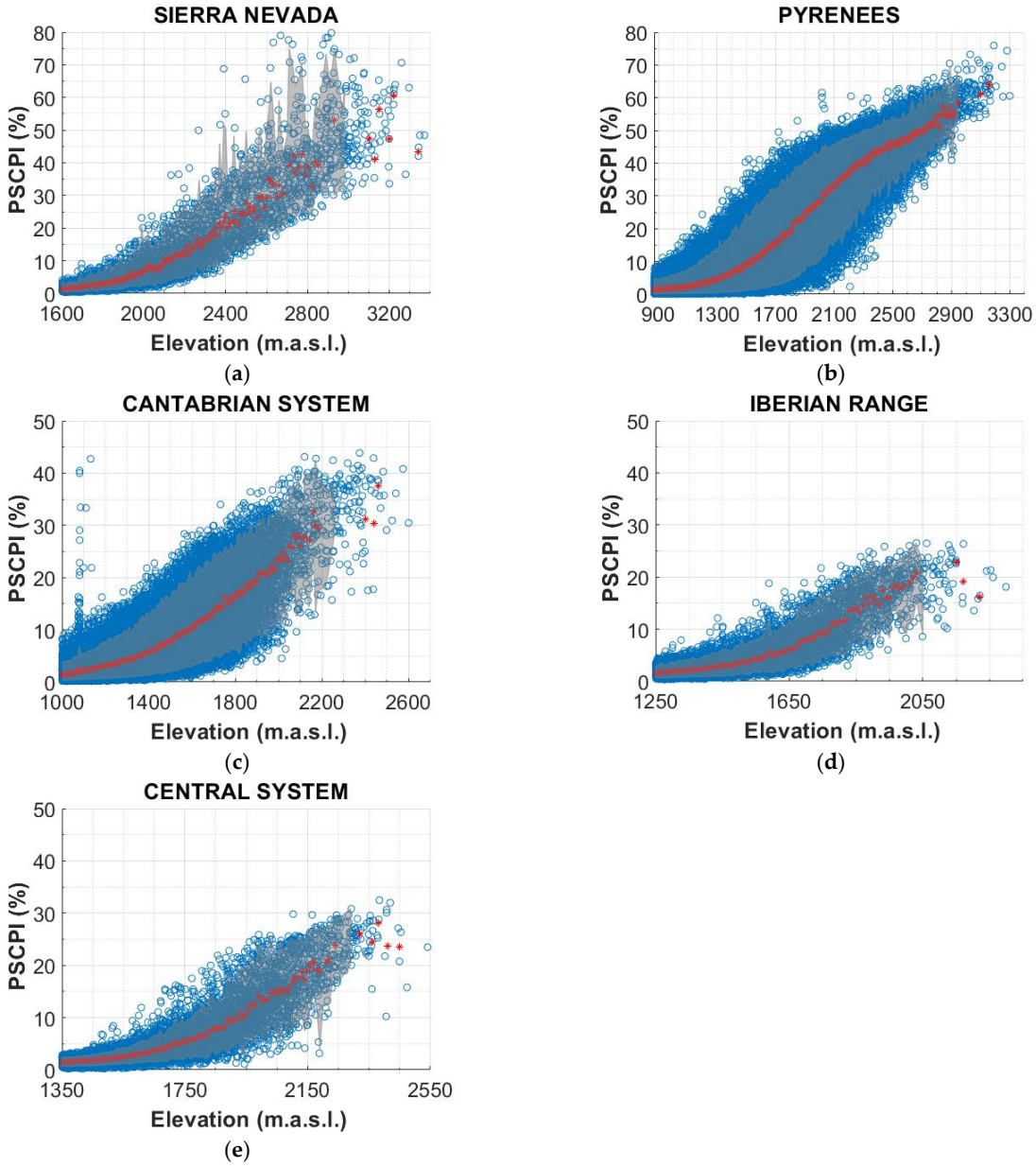

Figure 4. Distribution of the Probability of Snow Cover Presence Index (PSCPI) per elevation over the main mountain ranges of the Iberian Peninsula: (**a**) Sierra Nevada, (**b**) Pyrenees, (**c**) Cantabrian System, (**d**) Iberian Range and (**e**) Central System. The red color scatterplots indicate the average PSCPI per elevation. The shaded area represents PSCPI values within the confidence interval between 5% and 95%.

Furthermore, we analyzed the effect of latitude on snowpack assessing its correlation with snowline elevation under various average PSCPI thresholds. Our study reveals a consistent trend in lower snowline elevations as latitude increases (Figure 6). As expected, the Sierra Nevada consistently shows the highest snowline among the Iberian mountains, given its southernmost location within the Iberian Peninsula (latitude 37°). In contrast, the Pyrenees and the Cantabrian System exhibit the lowest snowline elevations, which is attributed to the fact that both mountainous regions are located at the highest and nearly identical latitudes (42.7° for the Cantabrian System and 42.6° for the Pyrenees). The Central System and the Iberian Range, situated at intermediate latitudes between the Sierra Nevada and the northern ranges (40.7° and 42°, respectively), display intermediate snowline elevations. Linear correlation analysis confirms a robust relationship between latitude

and snowline elevation as reflected in the high values of the determination coefficient ($R^2 \geq 0.84$) under the examined thresholds (Figure 6b). This underscores the significant influence of latitude on snow distribution patterns across the diverse montane regions of the Iberian Peninsula.

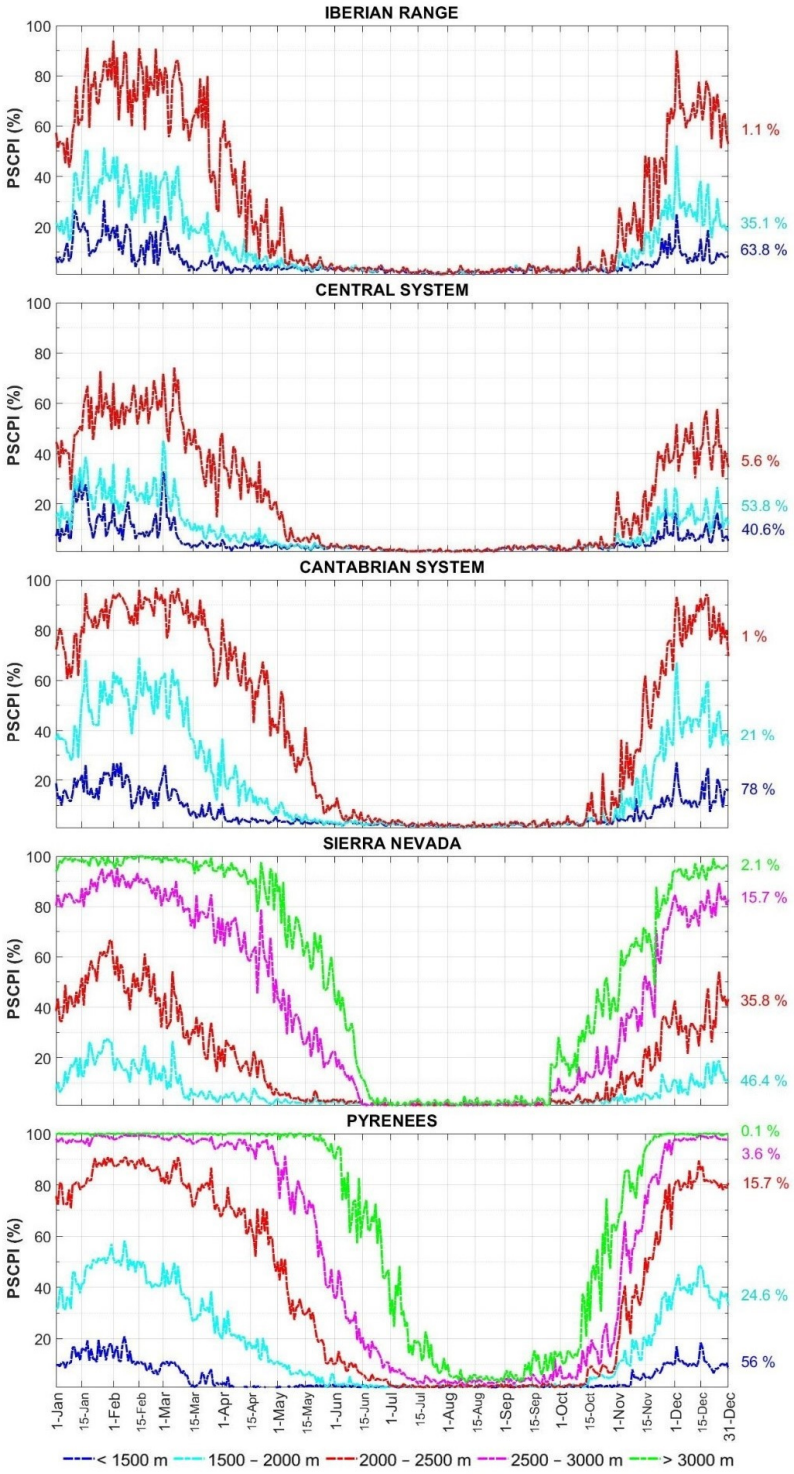

Figure 5. Daily distribution of the Probability of Snow Cover Presence Index (PSCPI) over the main Iberian mountains taking into account different elevation ranges. The right numbers indicate the percentage of area relative to the total area corresponding to each elevation band.

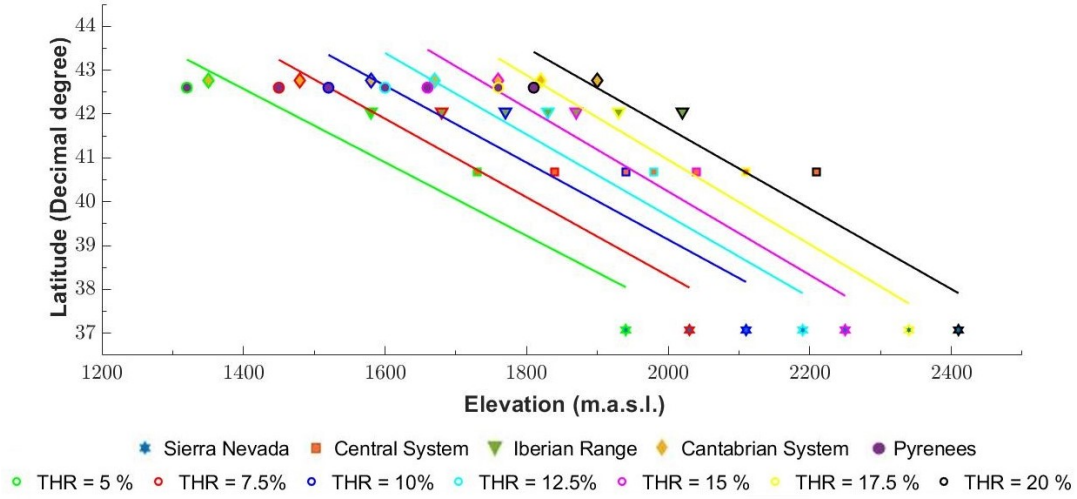

(**a**)

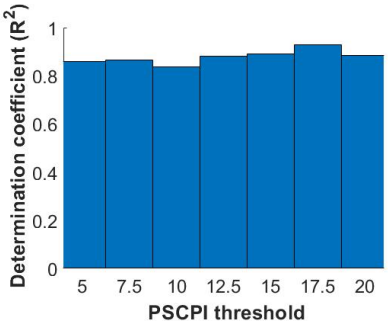

(**b**)

Figure 6. (**a**) Linear correlation between latitude and snowline elevation based on different thresholds (THR) of the average PSCPI over the main snow-dominated Iberian mountains; (**b**) Determination coefficient of the simple linear regression between latitude and snowline elevation associated with the examined average PSCPI thresholds.

4.2. Recent Impacts of Climate Change on Snow Cover

Figure 7 shows the temporal evolution of SCA for 5-year periods in terms of the average PSCPI for the entire domain of Iberian mountains. There exists a significative general trend in temporal inter-lustrum variability in the average PSCPI in winter months (December, January, and February). In these months, the first two lustra presented the greatest average PSCPI values, except in the case of February, where the third lustrum generally exhibited the highest average PSCPI of the time series. The last two lustra (2011–2015 and 2016–2020) over the 20-year period of study generally recorded the minimum average PSCPI values in all months of the snow season. Here, we plot the summer months for continuity on the graphs; however, they are not considered in the trend analysis.

Negative trends in SCA were observed over the 20-year period of study in the mountain ranges of the Iberian Peninsula (Table 1). Excluding April (in the Central System, Cantabrian System, and Iberian Range), February (in the Cantabrian System) and March (in the Pyrenees) negative rates in SCA were found in the snow season months. The largest decline in SCA rates occurred during December and January (Table 1). On the contrary, the smallest decline in SCA took place during April. In general, greater negative rates in SCA were observed in the Sierra Nevada over the snow season in relation to the other mountain ranges, except in December and April where the Central System (−4.45%/lustrum) and the Pyrenees (−0.99%/lustrum) revealed the greatest declines, respectively.

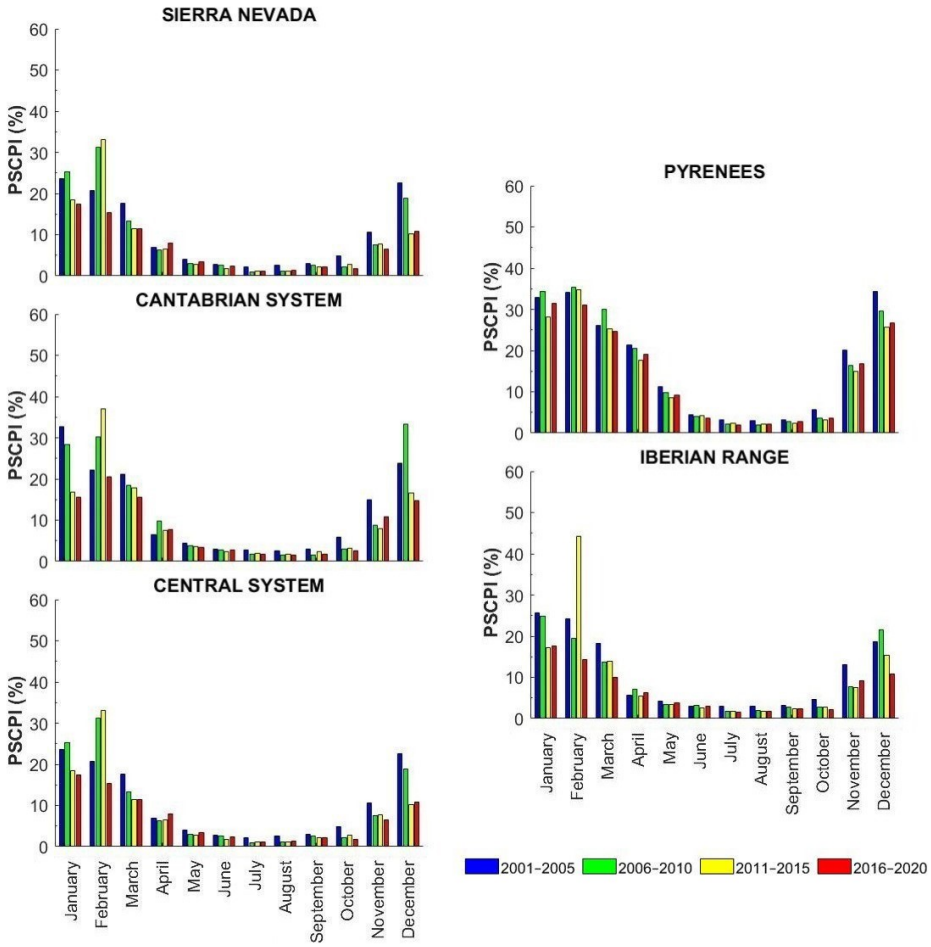

Figure 7. Five-year period temporal evolution of SCA in terms of the average PSCPI for the entire domain of the mountain ranges of the Iberian Peninsula on a monthly basis.

Table 1. Magnitude of the trend (%/lustrum) of the temporal changes in the Probability of Snow Cover Presence Index (PSCPI) of each month over the entire domain of the main-snow dominated mountain ranges of the Iberian Peninsula.

Month/Range	Sierra Nevada	Central System	Iberian Range	Cantabrian System	Pyrenees
November	−1.6	−1.17	−1.17	−1.12 [1]	−1.13
December	−2.71	−4.45	−2.98	−4.39	−2.65
January	−3.41	−2.54	−3.15	−6.26	−1.08
February	−1.9	−1.42	−0.51	+0.17	−0.99
March	−2.82	−2.06	−2.45	−1.76	+0.88
April	−0.6	+0.32	+0.04	+0.2	−0.99
May	−1.08	−0.18	−0.1	−0.33	−0.75

[1] Magnitude of the trend estimates with Sen's slope estimator (non-parametric method).

4.3. Potential of the Combined Use of SAR and MODIS for Snow Monitoring

An analysis of the contribution of SAR and MODIS to the total SCA and the PWSAI (defined as the probability of having a day with additional wet snow under cloud cover) was carried out in the Pyrenees (the only mountainous system of the Iberian Peninsula represented in the HRS&I SWS product) to evaluate the potential of SAR for the completion of optical SCA. The PWSAI consistently remains close to 100% throughout each month of the snow season (Figure 8a), indicating that nearly every day, the HRS&I product (wet snow) provides additional SCA information as regards MODIS. Only in November and December does the PWSAI slightly drop below 100%, highlighting SAR's potential to fill spatial gaps in SCA derived from optical sensors, specifically MODIS. Examining the

contribution of SCA relative to the total SCA, MODIS predominates during late autumn and winter (approximately 85% to 90%); however, the contribution from wet snow (HRS&I SWS) is notably significant (ranging from 10% to 15%) (Figure 8a). As the snowmelt season progresses, MODIS's contribution to the total SCA decreases considerably, while the contribution from HRS&I SWS (wet snow) begins to gain relevance, increasing significantly the supplied additional SCA information (27–40%). It is important to note that the HRS&I SWS contribution suddenly decreases in May (Figure 8a). This is due to the fact that, in the Pyrenees, the snowmelt phase mainly occurs during April, so that, in May, snow is predominantly restricted to higher elevations (above 2500 m.a.s.l.). At these elevations, temperatures frequently remain below 0 °C, which leads to a reduced contribution of wet snow relative to the total SCA. Figure 9 illustrates examples of SAR and MODIS data integration for SCA monitoring in the Pyrenees. The top panel shows an image from mid-winter, whereas the bottom panel shows an image from early spring.

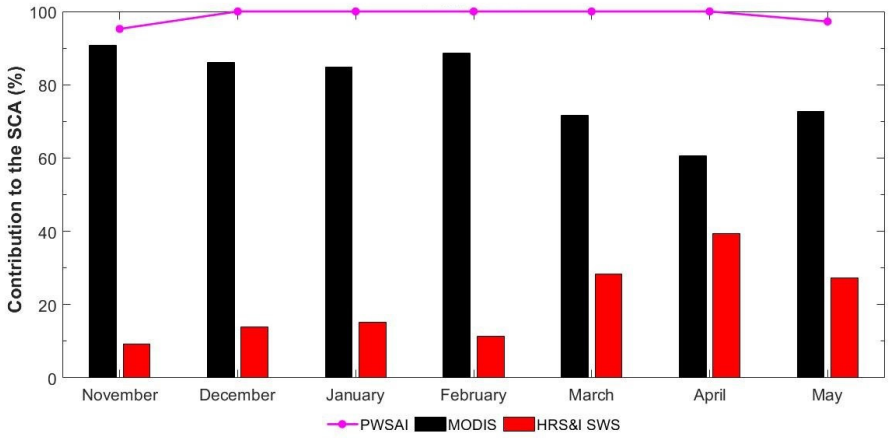

(**a**)

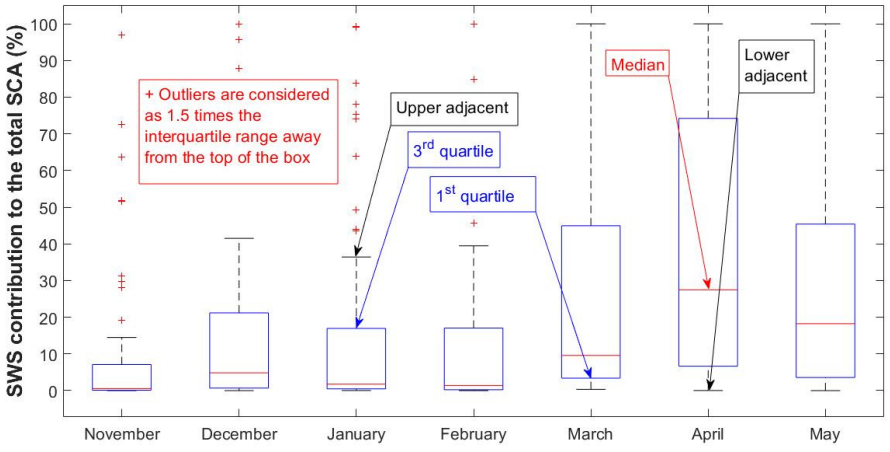

(**b**)

Figure 8. (**a**) Monthly PWSAI distribution and contribution of MODIS and HRS&I SWS (wet snow) products in relation to the total SCA over an average year in the Pyrenees. (**b**) Monthly variation of the contribution of HRS&I SWS product to the total SCA over an average year in the Pyrenees. The red line indicates the median, and the edges of the box (blue color) represent the first quartile (bottom edge) and third quartile (top edge). The upper adjacent is the furthest observation within one and a half times the interquartile range of the lower end of the box, and the upper adjacent is the furthest observation within one and a half times the interquartile range of the upper end of the box. Outliers are considered as the values greater than the upper adjacent.

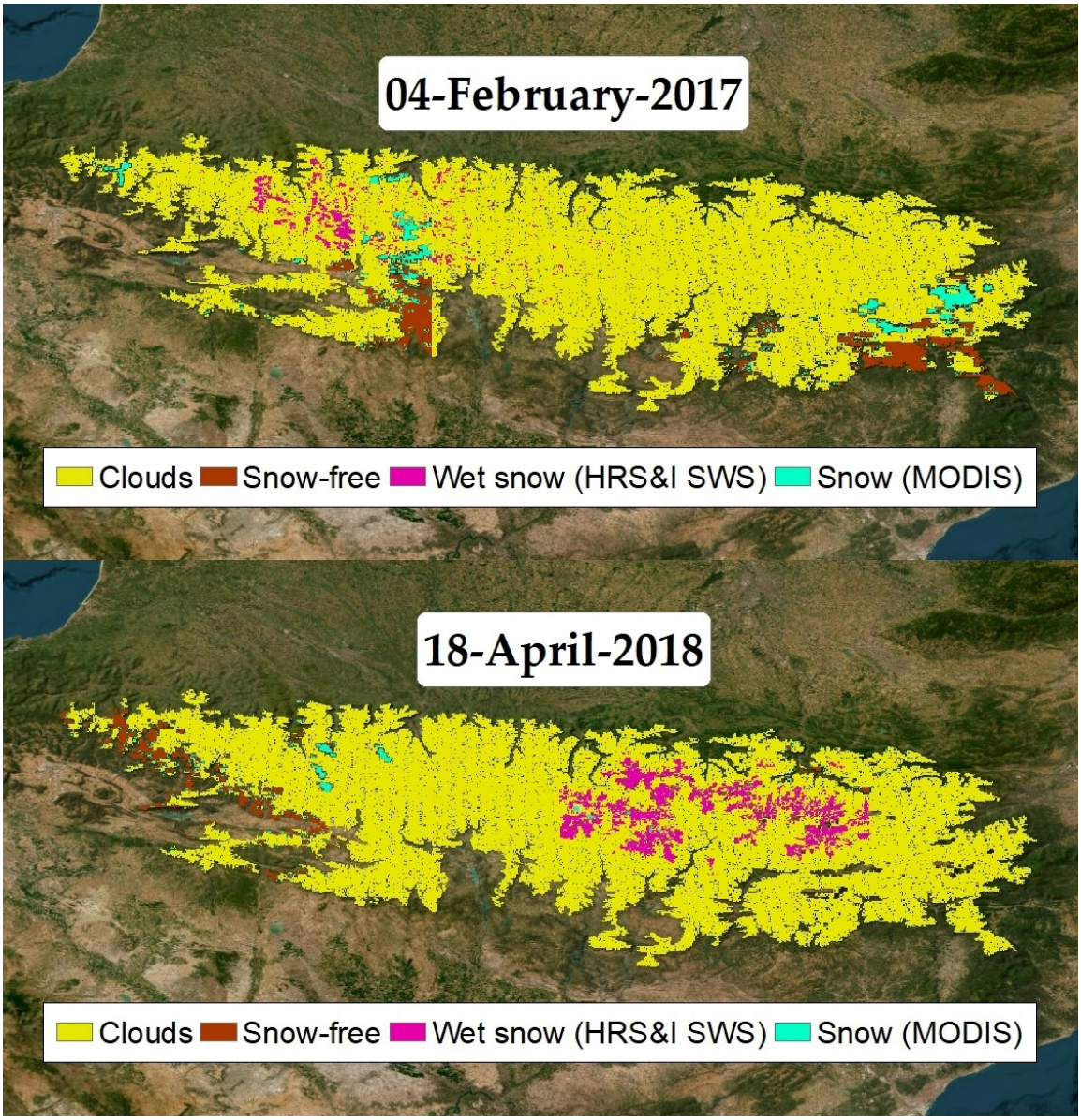

Figure 9. Examples of the combination of SAR (HRS&I SWS) and optical (MODIS) remote sensing products for the following dates: 04-February-2017 (winter) and 18-April-2018 (spring).

The evaluation of the additional SCA contribution provided by the HRS&I SWS product in the Pyrenees reveals relatively low variability during snow accumulation and stabilization phases but exhibits significant variations during snowmelt (Figure 8b). From late autumn through winter, the additional SCA contribution generally remains below 21%. Among these months, November exhibited the least variability (0.1–7.1%), while December showed the highest variation (0.5–17%). However, occasional outliers reaching peaks close to 100% were observed, indicating significant cloud cover on certain days. As mentioned earlier, the variability range widens notably during the snowmelt months (ranging from 3.4% to 74.2%) (Figure 8b).

5. Discussion

5.1. Potential Uncertainties of SAR and Optical Sensors for Snow Monitoring

Remote sensing data possess some uncertainties that should be considered for a proper interpretation of the presented results. MODIS products have limitations in snow and ice cloud classification [70]. Additionally, the presence of forest canopy in montane regions is

another source of uncertainty for SCA detection with optical and SAR remote sensing [71]. Furthermore, the PSCPI used in this research presents some limitations for a proper comparison among the Iberian mountains and the analysis of the temporal changes on SCA due to the differences in cloudiness distribution [72].

SCA monitoring through optical satellite sensors is primarily constrained by adverse weather conditions. Therefore, we conducted an assessment of the monthly cloud cover throughout an average year (see Figure A1). In this study, we found that the mountain ranges located at the north-central and northwestern quadrant of the Iberian Peninsula (Cantabrian System and Iberian Range) experienced the highest cloud cover during much of the snow season (PCPI ranging from 53% to 60%), surpassing the PCPI values of the Central System and the Pyrenees by around 4–5% and 10%, respectively. However, cloudiness was markedly reduced during the snowmelt phase, so that even in some months of the snowmelt season (May in the Cantabrian System and May and June in the case of the Central System), the cloud coverage in the Pyrenees was slightly higher. As expected, the Sierra Nevada consistently exhibited the lowest cloud cover during snow season (PCPI around 35% in winter and between 38% and 44% in spring). These findings are consistent with other studies that have identified maximum cloudiness in the Iberian Peninsula as being concentrated along the Atlantic-Cantabrian coastal area and the Pyrenees, mainly associated with large-scale northwesterly winds and the influence of cold fronts [73,74].

Both SAR and optical satellite sensors encounter limitations due to dense forest cover as it reduces the radar backscattering signal and obscures the underlying snowpack [75,76]. Dense forest areas are predominantly concentrated at lower elevations in the Iberian mountains and decrease progressively with elevation. In general, dense forest is sparse or non-existent at elevations where a seasonal snowpack exists, except in the case of the Pyrenees and the Iberian Range (Figure A2). These montane regions exhibited the greatest average TCD values (exceeding 50% at elevations below 1500 m.a.s.l. and 1730 m.a.s.l., respectively), whereas the Central System consistently displayed the least forest density (average TCD under 27%). The Sierra Nevada and the Cantabrian System also featured limited forest cover (average TCD around 30% below 2000 m.a.s.l. in the Sierra Nevada and about 35% below 1400 m.a.s.l. in the Cantabrian System).

5.2. Snow Characterization and Analysis of the Recent Climate Change Impacts on Snow Cover

Based on the analysis conducted in this study concerning the presence of snow in the Iberian mountains, our findings are congruent with other investigations [18,50]. The results presented here suggest a higher probability of snow presence in higher mountains, along with an extended snow season at higher elevations. In these regions, at higher and colder areas, snow melts later in the spring, and the depletion curve is rather steep due to increased shortwave radiation [77]. Our study found that snowmelt is mainly concentrated in spring in the Iberian mountains, although melting can occur in winter, with the snowpack often experiencing cycles of melting and accumulation. This finding aligns with previous research describing increased winter snowmelt associated with the recent climate change [78,79]. Moreover, Yang et al. [80] indicated that at mid-latitudes of Eurasia, snowmelt and snow accumulation occur simultaneously due to temperatures above 0 °C and high rainfall ratios. In the Iberian mountains, as in other temperate regions, snowpacks are consistently close to the zero-degree isotherm, thus, more sensitive to climate change impacts [81,82]. This research shows a general negative trend in snow cover throughout the snow season in the Iberian mountains, with the winter months (December and January) exhibiting the most pronounced decrease. Future climate projections forecast a warmer climate worldwide, with particularly significant warming trends in temperate mountains during the snow season [83]. This warming is expected to decrease melt rates in these regions [77], leading to an earlier-onset and slower snowmelt [79,84], and decreasing significatively the amount of accumulated snow and snow cover [85,86].

5.3. Potential of the Combined Use of SAR and Optical Remote Sensing for Snow Cover Mapping

The potential of active SAR as a complement to optical sensors for SCA mapping lies in its capability for wet snow dynamics monitoring [87]. Radar backscatter decreases and the one-way penetration depth of the radar signal drops drastically as liquid water content increases due to the high dielectric losses of water [88,89]. Radar signals at C- and X-band frequencies are reflected and scattered at the surface and within the uppermost centimeters of the snowpack due to liquid water content increase, whereas in the case of dry snow, the backscatter is strongly dominated by the contribution of the snow/ground interface [90]. Thus, it can be inferred that the use of active SAR for SCA mapping is primarily effective in snowmelt areas. Several studies have indicated the potential of combining SAR with optical sensors for SCA monitoring [91,92]. For instance, the Copernicus Land Cover Monitoring Service developed a gap-filled fractional SCA product by combining SAR (Sentinel-1) and optical (Sentinel-2) satellite constellations through spatial and temporal gap-filling over major European high mountain areas. An overall quality assessment of this product revealed a relatively consistent and good performance of HRS&I SWS for the spatial gap-filling of optical SCA throughout the snow season. This contrasts with our study's findings, which show a significant increase in the spatial gap-filling of MODIS SCA in spring compared to winter. These discrepancies can be attributed to the focus of our study on mid-latitude mountains, whereas the Copernicus assessment included both mid-latitude and high-latitude mountainous systems. Additionally, differences in the revisit times of the MODIS and Sentinel-2 sensors could explain the variations in the percentage of gap-filled optical SCA. Nonetheless, both studies suggest a high potential for the combined use of SAR and optical sensors.

In this research, we found that the Copernicus HRS&I SWS product provides a substantial amount of additional SCA data in Pyrenees in the spring season. Taking into account the sparse distribution of forest density in the main snow-dominated Iberian mountains, together with the different patterns observed in cloud coverage and the duration of the melting period, we can infer that wet snow (HRS&I SWS product) could contribute even more significantly to additional SCA information in the Sierra Nevada. In contrast, the contribution is expected to be less in the Cantabrian system, Central System, and Iberian Range. However, a more comprehensive analysis is needed to evaluate the contribution of wet snow to the SCA dynamics in the rest of the mountain ranges of the Iberian Peninsula. This analysis should consider other snow variables such as snow depth or snow water equivalent to provide more detailed understanding.

6. Conclusions

We evaluated the spatiotemporal distribution of SCA in relation to elevation and location over the main snow-dominated montane regions of the Iberian Peninsula. The Pyrenees and the Sierra Nevada display long-lasting snowpack behaviors (275 days and 244 days, respectively) related to the higher elevations existing in these mountains compared to the Cantabrian, Central, and Iberian Ranges. In the Iberian mountains, snow melting primarily occurs in the spring season. Elevation plays a crucial role in the onset of the snowmelt, with higher elevations undergoing later snow melting due to colder temperatures, which explains the long-lasting snowpack observed in the Pyrenees and the Sierra Nevada. Furthermore, we found that the snowline elevation, which determines the presence of a regular snowpack along the snow season, is strongly influenced by the latitudinal gradient ($R^2 \geq 0.84$). However, it is worth noting that other geographical factors such as the distance from the Atlantic Ocean and continentality also play important roles. Additionally, we assessed the recent impacts of climate change on SCA and found a general negative trend across all snow season months. The decline in SCA was particularly significant during the winter months (December and January). We also evaluated the potential use of SAR as a complement for the SCA spatial gap-filling of optical sensors (MODIS). Our analysis in the Pyrenees demonstrates the high potential of the combined use of SAR and MODIS, especially in spring, with proportions of wet snow contributing to

the total SCA ranging from 27.2% to 39.4% between March and May. Based on these results, we can conclude that in the rest of the Iberian mountains, where the Copernicus HRS&I SWS product is not currently available, wet snow can provide valuable additional SCA information when used in conjunction with optical sensors. Therefore, the development of the HRS&I SWS product for the Cantabrian System, Central System, Iberian Range, and Sierra Nevada represents a dynamic and engaging future line of research.

Author Contributions: Conceptualization, D.P.-V. and A.-J.C.-L.; methodology, D.P.-V.; software, J.-D.H.-H. and C.H.; validation, D.P.-V., A.-J.C.-L. and S.R.F.; formal analysis, J.-D.H.-H.; investigation, J.-D.H.-H.; data curation, J.-D.H.-H.; writing—original draft preparation, J.-D.H.-H.; writing—review and editing, D.P.-V., A.-J.C.-L., and S.R.F.; visualization, J.-D.H.-H.; supervision, D.P.-V. and A.-J.C.-L.; project administration, D.P.-V.; funding acquisition, D.P.-V. and A.-J.C.-L. All authors have read and agreed to the published version of the manuscript.

Funding: This research was funded by the following projects: STAGES-IPCC (TED2021-130744B-C21/AEI/10.13039/501100011033/Unión Europea NextGenerationEU/PRTR), SIGLO-PRO (PID2021-128021OB-I00/AEI/10.13039/501100011033/FEDER, UE), from the Spanish Ministry of Science, Innovation and Universities, SER-PM (2908/22; Organismo Autónomo Parques Nacionales) from the National Park Research Program, and SIERRA-CC (PID2022-137623OA-I00) funded by MICIU/AEI/10.13039/501100011033 and by FEDER, UE. Fassnacht S. R. was a Fulbright Global Scholar at CSIC-IGME during this work.

Data Availability Statement: The AEMET 5 km climate dataset is available on the official AEMET website: https://www.aemet.es/es/serviciosclimaticos/cambio_climat/datos_diarios?w=2 (accessed on 21 June 2023). The MODIS Terra Snow Cover Collection 6 product is available on the MODIS webpage: https://modis.gsfc.nasa.gov/data/ (accessed on 15 May 2023). The High-Resolution Snow and Ice SAR wet snow product is available to download from Copernicus Land Monitoring Service: https://land.copernicus.eu/en/products/snow/high-resolution-sar-wet-snow (accessed on 29 July 2023). Likewise, the High-Resolution Layer Tree Cover Density is available to download from Copernicus Land Monitoring Service: https://land.copernicus.eu/en/products/high-resolution-layer-tree-cover-density/tree-cover-density-2018 (accessed on 5 September 2023).

Conflicts of Interest: The authors declare no conflicts of interest.

Appendix A. Generalized Methods and Limitations of Optical and Radar Sensors for Snow Cover Mapping

The effectiveness of optical spaceborne sensors in detecting snow cover is largely due to the high reflectivity (albedo) of snow compared to other Earth's surface materials [93]. These sensors typically operate using multispectral bands, including visible light, infrared, and thermal. The most common method for snow cover identification employs the NDSI, which leverages spectral information from the visible (green) and near-infrared bands [94,95]:

$$NDSI = \frac{\sigma_{green} - \sigma_{infrared}}{\sigma_{green} + \sigma_{infrared}} \quad \text{(A1)}$$

where σ denotes the reflectance in a specific wavelength band of the electromagnetic spectrum. Cloud cover and dense forests present significant obstacles to operational snow cover monitoring [96]. A notable limitation is that the snow surface is often completely obscured from the satellite sensor's view by clouds. Another common problem in optical multispectral imagery is the confusion between snow and ice-clouds [97]. Additionally, in densely forested areas, particularly coniferous forests, the reflectance in the green band is highly sensitive to increases in canopy cover (high canopy cover values can cause negative NDSI values in snow-covered areas), making accurate snow cover classification in such regions challenging [98].

Wet snow monitoring with SAR remote sensing is based on the ratio of backscattering coefficient between one wet snow image and a reference image that represents the typical backscattering conditions of snow-free and dry snow surfaces. Nagler et al. [40] determined that a threshold of −3 dB provides a good accuracy for wet snow classification. Recently,

a more efficient method for wet snow mapping was developed by means of the fusion of backscattering coefficients ratios from co-polarization and cross-polarization signals [30], so that in this instance established as optimal a −2 dB threshold for the combined backscattering ratio. However, it has been shown that these fixed thresholds (−2 dB and −3 dB) may not be suitable under certain land cover uses (agricultural, forested, urban areas, etc.), incidence angles and snow wetness conditions [99,100].

In active-microwave remote sensing with L-, C-, or X-band forest canopy above wet snow typically increases the backscattering coefficient due to volume scattering within the canopy. This effect reduces the ratio of the backscattering coefficient between wet snow and snow-free or dry snow surfaces [99]. Conversely, in passive-microwave remote sensing, forest canopy attenuates backscattering signal from snow and ground, while adding its own contribution [101]. Additionally, Baghdadi et al. [102] demonstrated that the backscattering coefficient of wet snow is strongly dependent on the snow-surface roughness and the incidence angle. It was also found that very high liquid-water content within the snowpack could reduce the differences between the backscattering coefficients of wet and dry snow or snow-free conditions.

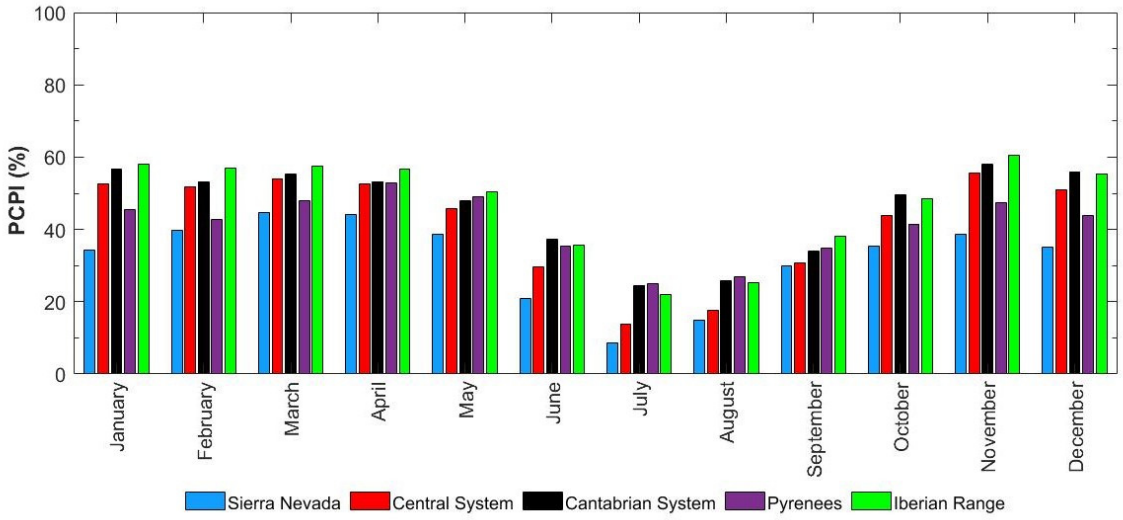

Figure A1. Monthly distribution of the Probability of Cloud Presence Index (PCPI) for an average year over the main Iberian mountains.

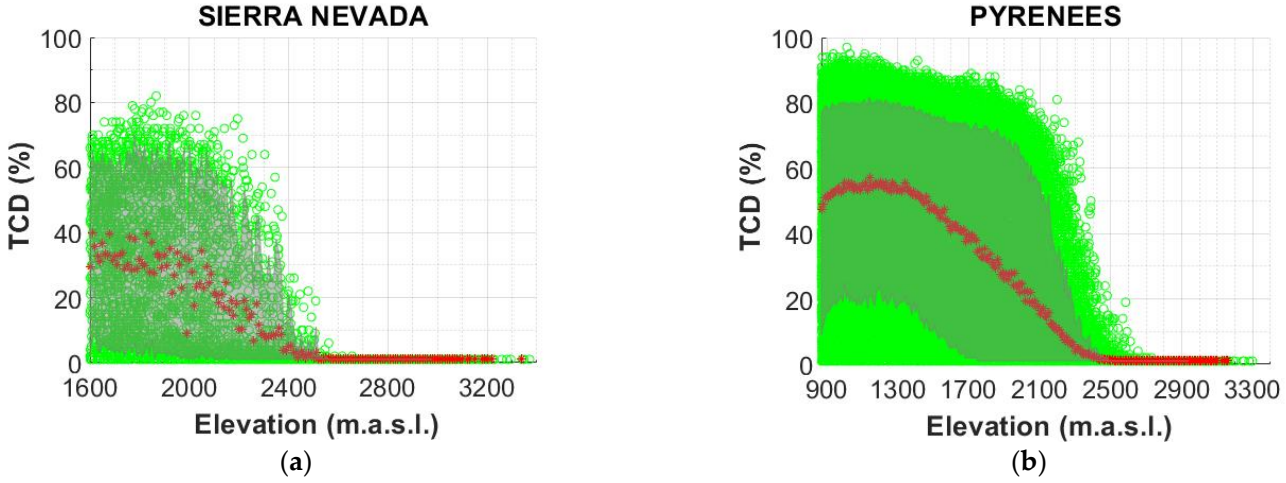

Figure A2. *Cont.*

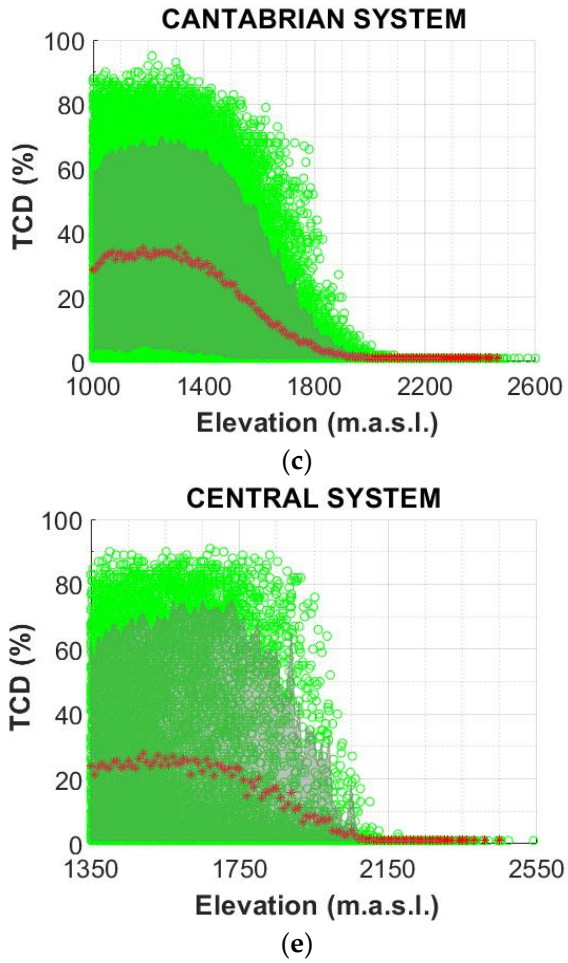

Figure A2. Distribution of the tree-cover density (TCD) per elevation over the main mountain ranges of the Iberian Peninsula: (**a**) Sierra Nevada, (**b**) Pyrenees, (**c**) Cantabrian System, (**d**) Iberian Range, and (**e**) Central System. The red color scatterplots indicate the average TCD per elevation. The shaded area represents TCD values within the confidence interval between 10% and 90%.

References

1. Vavrus, S. The role of terrestrial snow cover in the climate system. *Clim. Dyn.* **2007**, *29*, 73–88. [CrossRef]
2. Yeh, T.C.; Wetherald, R.T.; Manabe, S. A model study of the short-term climatic and hydrologic effects of sudden snow-cover removal. *Mon. Weather Rev.* **1983**, *111*, 1013–1024. [CrossRef]
3. Biemans, H.; Siderius, C.; Lutz, A.F.; Nepal, S.; Ahmad, B.; Hassan, T.; von Bloh, W.; Wijngaard, R.R.; Wester, P.; Shrestha, A.B.; et al. Importance of snow and glacier meltwater for agriculture on the Indo-Gangetic Plain. *Nat. Sustain.* **2019**, *2*, 594–601. [CrossRef]
4. Qin, Y.; Abatzoglou, J.T.; Siebert, S.; Huning, L.S.; Agha Kouchak, A.; Mankin, J.S.; Hong, C.; Tong, D.; Davis, S.J.; Mueller, N.D. Agricultural risks from changing snowmelt. *Nat. Clim. Chang.* **2020**, *10*, 459–465. [CrossRef]
5. Groffman, P.M.; Driscoll, C.T.; Fahey, T.J.; Hardy, J.P.; Fitzhugh, R.D.; Tierney, G.L. Colder soils in a Warmer World: A snow manipulation study in a northern hardwood forest ecosystem. *Biogeochemistry* **2011**, *56*, 135–150. [CrossRef]
6. Pauli, J.N.; Zuckerberg, B.; Whiteman, J.P.; Porter, W. The subnivium: A deteriorating seasonal refugium. *Front. Ecol. Environ.* **2013**, *11*, 260–267. [CrossRef]
7. Niittynen, P.; Heikkinen, R.K.; Luoto, M. Snow cover is a neglected driver of Arctic biodiversity loss. *Nat. Clim. Chang.* **2018**, *8*, 997–1001. [CrossRef]
8. Harrison, S.J.; Winterbottom, S.J.; Johnson, R.C. A preliminary assessment of the socio-economic and environmental impacts of recent changes in winter snow cover in Scotland. *Scott. Geogr. J.* **2001**, *117*, 297–312. [CrossRef]
9. Yang, Y.; Wu, X.-J.; Liu, S.-W.; Xiao, C.-D.; Wang, X. Valuating service loss of snow cover in Irtysh River Basin. *Adv. Clim. Chang. Res.* **2019**, *10*, 109–114. [CrossRef]
10. Wu, X.; Wang, X.; Liu, S.; Yang, Y.; Xu, G.; Xu, Y.; Jiang, T.; Xiao, C. Snow cover loss compounding the future economic vulnerability of western China. *Sci. Total Environ.* **2021**, *755*, 143025. [CrossRef]

11. Moreno-Gené, J.; Sánchez-Pulido, L.; Cristobal-Fransi, E.; Daries, N. The Economic Sustainability of Snow Tourism: The Case of Ski Resorts in Austria, France, and Italy. *Sustainability* **2018**, *10*, 3012. [CrossRef]
12. Moreno-Gené, J.; Daries, N.; Cristóbal-Fransi, E.; Sánchez-Pulido, L. Snow tourism and economic sustainability: The financial situation of ski resorts in Spain. *Appl. Econ.* **2020**, *52*, 5726–5744. [CrossRef]
13. Parthum, B.; Christensen, P. A market for snow: Modeling winter recreation patterns under current and future climate. *J. Environ. Econ. Manag.* **2022**, *113*, 102637. [CrossRef] [PubMed]
14. Kulkarni, A.V.; Randhawa, S.S.; Rathore, B.P.; Bahuguna, I.M.; Sood, R.K. Snow and glacier melt runoff model to estimate hydropower potential. *J. Indian Soc. Remote Sens.* **2002**, *30*, 221–228. [CrossRef]
15. Bombelli, G.M.; Soncini, A.; Bianchi, A.; Bocchiola, D. Potentially modified hydropower production under climate change in the Italian Alps. *Hydrol. Process.* **2019**, *33*, 2355–2372. [CrossRef]
16. Collados-Lara, A.-J.; Pardo-Igúzquiza, E.; Pulido-Velazquez, D. A distributed cellular automata model to simulate potential future impacts of climate change on snow cover area. *Adv. Water Resour.* **2019**, *124*, 106–119. [CrossRef]
17. Collados-Lara, A.-J.; Pulido-Velazquez, D.; Pardo-Igúzquiza, E.; Alonso-González, E. Estimation of the spatiotemporal dynamic of snow water equivalent at mountain range scale under data scarcity. *Sci. Total Environ.* **2020**, *741*, 140485. [CrossRef]
18. Collados-Lara, A.-J.; Pardo-Igúzquiza, E.; Pulido-Velazquez, D. Assessing the impact of climate change—and its uncertainty—on snow cover areas by using cellular automata models and stochastic weather generators. *Sci. Total Environ.* **2021**, *788*, 147776. [CrossRef]
19. Pardo-Igúzquiza, E.; Collados-Lara, A.-J.; Pulido-Velazquez, D. Estimation of the spatiotemporal dynamics of snow covered area by using cellular automata models. *J. Hydrol.* **2017**, *550*, 230–238. [CrossRef]
20. Collados-Lara, A.-J.; Pardo-Igúzquiza, E.; Pulido-Velazquez, D. Spatiotemporal estimation of snow depth using point data from snow stakes, digital terrain models, and satellite data. *Hydrol. Process.* **2017**, *31*, 1966–1982. [CrossRef]
21. Collados-Lara, A.-J.; Pardo-Igúzquiza, E.; Pulido-Velazquez, D. Optimal design of snow stake networks to estimate snow depth in an alpine mountain range. *Hydrol. Process.* **2020**, *34*, 82–95. [CrossRef]
22. Jimeno-Sáez, P.; Pulido-Velazquez, D.; Collados-Lara, A.-J.; Pardo-Igúzquiza, E.; Senent-Aparicio, J.; Baena-Ruiz, L. A preliminary assessment of the "undercatching" and the precipitation pattern in an alpine basin. *Water* **2020**, *12*, 1061. [CrossRef]
23. Alvarado-Montero, R.; Uysal, G.; Collados-Lara, A.-J.; Arda Şorman, A.; Pulido-Velazquez, D.; Şensoy, A. Comparison of sequential and variational assimilation methods to improve hydrological predictions in snow dominated mountainous catchments. *J. Hydrol.* **2022**, *612*, 127981. [CrossRef]
24. Dietz, A.J.; Kuenzer, C.; Dech, S. Global SnowPack: A new set of snow cover parameters for studying status and dynamics of the planetary snow cover extent. *Remote Sens. Let.* **2015**, *6*, 844–853. [CrossRef]
25. Dedieu, J.; Lessard-Fontaine, A.; Ravazzani, G.; Cremonese, E.; Shalpykova, G.; Beniston, M. Shifting mountain snow patterns in a changing climate from remote sensing retrieval. *Sci. Total Environ.* **2014**, *493*, 1267–1279. [CrossRef] [PubMed]
26. Notarnicola, C. Hotspots of snow cover changes in global mountain regions over 2000–2018. *Remote Sens. Environ.* **2020**, *243*, 111781. [CrossRef]
27. Hori, M.; Sugiura, K.; Kobayashi, K.; Aoki, T.; Tanikawa, T.; Kuchiki, K.; Niwano, M.; Enomoto, H. A 38-year (1978–2015) Northern Hemisphere daily snow cover extent product derived using consistent objective criteria from satellite-borne optical sensors. *Remote Sens. Environ.* **2017**, *191*, 402–418. [CrossRef]
28. Tekeli, A.E.; Akyürek, Z.; Arda Şorman, A.; Şensoy, A.; Ünal Şorman, A. Using MODIS snow cover maps in modeling snowmelt runoff process in the eastern part of Turkey. *Remote Sens. Environ.* **2005**, *97*, 216–230. [CrossRef]
29. Brakenridge, R.; Anderson, E. Modis-based flood detection, mapping and measurement: The potential for operational hydrological applications. In *Nato Science Series: IV: Earth and Environmental Sciences*; Marsalek, J., Stancalie, G., Balint, G., Eds.; Kluwer Academic Publishers: Dordrecht, The Netherlands, 2006; Volume 72, pp. 1–12.
30. Hammond, J.C.; Saavedra, F.A.; Kampf, S.K. How does snow persistence relate to annual streamflow in mountain watersheds of the western U.S. with wet maritime and dry continental climates? *Water Resour. Res.* **2018**, *54*, 2605–2623. [CrossRef]
31. Hall, D.K.; Riggs, G.A. Accuracy assessment of the MODIS snow products. *Hydrol. Process.* **2007**, *21*, 1534–1547. [CrossRef]
32. Hall, D.K.; Foster, J.L.; Chang, A.T.C.; Benson, C.S.; Chien, J.Y.L. Determination of snow-covered area in different land covers in central Alaska, U.S.A. from aircraft data—April 1995. *Ann. Glaciol.* **1998**, *26*, 149–155. [CrossRef]
33. Prudente, V.H.R.; Martins, V.S.; Vieira, D.C.; e Silva, N.R.D.F.; Adami, M.; Sanches, I.D.A. Limitations of cloud cover for optical remote sensing of agricultural areas across South America. *Remote Sens. Appl.* **2020**, *20*, 100414. [CrossRef]
34. Huang, Y.; Song, Z.; Yang, H.; Yu, B.; Liu, H.; Che, T.; Chen, J.; Wu, J.; Shu, S.; Peng, X.; et al. Snow cover detection in mid-latitude mountainous and polar regions using nighttime light data. *Remote Sens. Environ.* **2022**, *268*, 112766. [CrossRef]
35. Hu, K.; Zhang, E.; Xia, M.; Weng, L.; Lin, H. MCANet: A Multi-Branch Network for Cloud/Snow Segmentation in High-Resolution Remote Sensing Images. *Remote Sens.* **2023**, *15*, 1055. [CrossRef]
36. Liu, C.; Li, Z.; Zhang, P.; Huang, L.; Li, Z.; Gao, S. Wet snow detection using dual-polarized Sentinel-1 SAR time series data considering different land categories. *Geocarto Int.* **2022**, *37*, 10907–10924. [CrossRef]
37. Karbou, F.; Veyssière, G.; Coleou, C.; Dufour, A.; Gouttevin, I.; Durand, P.; Gascoin, S.; Grizonnet, M. Monitoring Wet Snow Over an Alpine Region Using Sentinel-1 Observations. *Remote Sens.* **2021**, *13*, 381. [CrossRef]
38. Tsai, N.; Dietz, N.; Oppelt, N.; Kuenzer, N. Wet and Dry Snow Detection Using Sentinel-1 SAR Data for Mountainous Areas with a Machine Learning Technique. *Remote Sens.* **2019**, *11*, 895. [CrossRef]

39. Wagner, W.; Blöschl, G.; Pampaloni, P.; Calvet, J.; Bizzarri, B.; Wigneron, J.; Kerr, Y. Operational readiness of microwave remote sensing of soil moisture for hydrologic applications. *Hydrol. Res.* **2007**, *38*, 1–20. [CrossRef]
40. Nagler, T.; Rott, H. Retrieval of wet snow by means of multitemporal SAR data. *IEEE Trans. Geosci. Remote Sens.* **2000**, *38*, 754–765. [CrossRef]
41. Nagler, T.; Rott, H.; Ripper, E.; Bippus, G.; Hetzenecker, M. Advancements for snowmelt monitoring by means of sentinel-1 SAR. *Remote Sens.* **2016**, *8*, 348. [CrossRef]
42. Rees, W.G. Physical Properties of Snow and Ice. In *Book Remote Sensing of Snow and Ice*, 1st ed.; CRC Press Books: Boca Raton, FL, USA, 2005; pp. 99–136. [CrossRef]
43. Mätzler, C.; Schanda, E. Snow mapping with active microwave sensors. *Int. J. Remote Sens.* **1984**, *5*, 409–422. [CrossRef]
44. Rott, H. Prospects of microwave remote sensing for snow hydrology. In Proceedings of the Cocoa Beach Workshop, Cocoa Beach, FL, USA, 19–23 August 1985.
45. Rott, H.; Mätzler, C. Possibilities and Limits of Synthetic Aperture Radar for Snow and Glacier Surveying. *Ann. Glaciol.* **1987**, *9*, 195–199. [CrossRef]
46. Attema, E.; Davidson, M.; Snoeij, P.; Rommen, B.; Floury, N. Sentinel-1 mission overview. In Proceedings of the 2009 IEEE International Geoscience and Remote Sensing Symposium, Cape Town, South Africa, 12–17 July 2009. [CrossRef]
47. Pulido-Velazquez, D.; Collados-Lara, A.J.; Alcalá, F.J. Assessing impacts of future potential climate change scenarios on aquifer recharge in continental Spain. *J. Hydrol.* **2018**, *567*, 803–819. [CrossRef]
48. Lopez-Bustins, J.A.; Martin-Vide, J.; Sanchez-Lorenzo, A. Iberia winter rainfall trends based upon changes in teleconnection and circulation patterns. *Glob. Planet. Chang.* **2008**, *63*, 171–176. [CrossRef]
49. Castro, M.D.; Martín-Vide, J.; Alonso Oroza, S. El clima de España: Pasado, presente y escenarios de clima para el siglo XXI. In *Evaluación Preliminar de los Impactos en España por Efecto del Cambio Climático*; Ministerio de Medio Ambiente: Madrid, Spain, 2005; pp. 1–64.
50. Alonso-González, E.; López-Moreno, J.I.; Navarro-Serrano, F.; Sanmiguel-Vallelado, A.; Revuelto, J.; Domínguez-Castro, F.; Ceballos, A. Snow climatology for the mountains in the Iberian Peninsula using satellite imagery and simulations with dynamically downscaled reanalysis data. *Int. J. Climatol.* **2019**, *40*, 477–491. [CrossRef]
51. Dozier, J. Spectral signature of alpine snow cover from the Landsat thematic mapper. *Remote Sens. Environ.* **1989**, *28*, 9–22. [CrossRef]
52. Salomonson, V.V.; Appel, I. Estimating fractional snow cover from MODIS using the normalized difference snow index. *Remote Sens. Environ.* **2004**, *89*, 351–360. [CrossRef]
53. Salomonson, V.V.; Appel, I. Development of the Aqua MODIS NDSI fractional snow cover algorithm and validation results. *IEEE Trans. Geosci. Remote Sens.* **2006**, *44*, 1747–1756. [CrossRef]
54. Härer, S.; Bernhardt, M.; Siebers, M.; Schulz, K. On the need for a time- and location-dependent estimation of the NDSI threshold value for reducing existing uncertainties in snow cover maps at different scales. *Cryosphere* **2018**, *12*, 1629–1642. [CrossRef]
55. Tong, R.; Parajka, J.; Komma, J.; Blöschl, G. Mapping snow cover from daily Collection 6 MODIS products over Austria. *J. Hydrol.* **2020**, *590*, 125548. [CrossRef]
56. Déry, S.J.; Brown, R.D. Recent Northern Hemisphere snow cover extent trends and implications for the snow-albedo feedback. *Geophys. Res. Lett.* **2007**, *34*. [CrossRef]
57. Sen, P.K. Estimates of the Regression Coefficient Based on Kendall's Tau. *J. Am. Stat. Assoc.* **1968**, *63*, 1379–1389. [CrossRef]
58. Anderson, T.W.; Darling, D.A. Asymptotic Theory of Certain «Goodness of Fit» Criteria Based on Stochastic Processes. *Ann. Math. Stat.* **1952**, *23*, 193–212. [CrossRef]
59. Anderson, T.W.; Darling, D.A. A Test of Goodness of Fit. *J. Am. Stat. Assoc.* **1954**, *49*, 765. [CrossRef]
60. Peral García, M.C.; Navascués, B.; Ramos Calzado, P. Serie de precipitación diaria en rejilla con fines climáticos. In *Nota Técnica 24 de AEMET*; AEMET: Madrid, Spain, 2017. [CrossRef]
61. Amblar-Francés, M.P.; Ramos-Calzado, P.; Sanchis-Lladó, J.; Hernanz-Lázaro, A.; Peral-García, M.C.; Navascués, B.; Dominguez-Alonso, M.; Pastor-Saavedra, M.A.; Rodríguez-Camino, E. High resolution climate change projections for the Pyrenees region. *Adv. Sci. Res.* **2020**, *17*, 191–208. [CrossRef]
62. Gómez-Gómez, J.D.; Pulido-Velazquez, D.; Collados-Lara, A.J.; Fernandez-Chacon, F. The impact of climate change scenarios on droughts and their propagation in an arid Mediterranean basin. A useful approach for planning adaptation strategies. *Sci. Total Environ.* **2022**, *820*, 153128. [CrossRef] [PubMed]
63. Hidalgo-Hidalgo, J.D.; Collados-Lara, A.J.; Pulido-Velazquez, D.; Rueda-Valdivia, F.J.; Pardo-Igúzquiza, E. Analysis of the Potential Impacts of Climate Change on climatic droughts, snow dynamics and the correlation between them. *Water* **2022**, *14*, 1081. [CrossRef]
64. Collados-Lara, A.J.; Gómez-Gómez, J.D.; Pulido-Velazquez, D.; Pardo-Igúzquiza, E. An approach to identify the best climate models for the assessment of climate change impacts on meteorological and hydrological droughts. *Nat. Hazards Earth Syst. Sci.* **2022**, *22*, 599–616. [CrossRef]
65. Collados-Lara, A.J.; Pardo-Igúzquiza, E.; Pulido-Velazquez, D.; Jiménez-Sánchez, J. Precipitation fields in an alpine Mediterranean catchment: Inversion of precipitation gradient with elevation or undercatch of snowfall? *Int. J. Climatol.* **2018**, *38*, 3565–3578. [CrossRef]

66. Collados-Lara, A.J.; Fassnacht, S.R.; Pardo-Igúzquiza, E.; Pulido-Velazquez, D. Assessment of high-resolution air temperature fields at Rocky Mountain National Park by combining scarce point measurements with elevation and remote sensing data. *Remote Sens.* **2020**, *13*, 113. [CrossRef]
67. Collados-Lara, A.J.; Fassnacht, S.R.; Pulido-Velazquez, D.; Pfohl, A.K.D.; Morán-Tejeda, E.; Venable, N.B.H.; Pardo-Igúzquiza, E.; Puntenney-Desmond, K. Intra-day variability of temperature and its near-surface gradient with elevation over mountainous terrain: Comparing MODIS land surface temperature data with coarse and fine scale near-surface measurements. *Int. J. Climatol.* **2021**, *41*, E1435–E1449. [CrossRef]
68. Jones, P.D.; Hulme, M. Calculating regional climatic time series for temperature and precipitation: Methods and illustrations. *Int. J. Climatol.* **1996**, *16*, 361–377. [CrossRef]
69. Riggs, G.A.; Hall, D.K.; Roman, M.O. *MODIS Snow Products Collection 6 User Guide*; National Snow and Ice Data Center: Boulder, CO, USA, 2019. Available online: https://modis-snow-ice.gsfc.nasa.gov/ (accessed on 25 May 2023).
70. Wang, T.; Fetzer, E.J.; Wong, S.; Kahn, B.H.; Yue, Q. Validation of MODIS cloud mask and multilayer flag using CloudSat-CALIPSO cloud profiles and a cross-reference of their cloud classifications. *J. Geophys. Res.* **2016**, *121*, 11620–11635. [CrossRef]
71. Simic, A.; Fernandes, R.; Brown, R.; Romanov, P.; Park, W.; Hall, D.K. Validation of MODIS, VEGETATION, and GOES+SSM/I snow cover products over Canada based on surface snow depth observations. In Proceedings of the IEEE International Geoscience and Remote Sensing Symposium, Toulouse, France, 21–25 July 2003. [CrossRef]
72. Royé, D.; Lorenzo, N.; Rasilla, D.; Martí, A. Spatio-temporal variations of cloud fraction based on circulation types in the Iberian Peninsula. *Int. J. Climatol.* **2019**, *39*, 1716–1732. [CrossRef]
73. Azorin-Molina, C.; Baena-Calatrava, R.; Echave-Calvo, I.; Connell, B.H.; Vicente-Serrano, S.M.; López-Moreno, J.I. A daytime over land algorithm for computing AVHRR convective cloud climatologies for the Iberian Peninsula and the Balearic Islands. *Int. J. Climatol.* **2012**, *33*, 2113–2128. [CrossRef]
74. Azorin-Molina, C.; Vicente Serrano, S.M.; Chen, D.; Connell, B.H.; Domínguez-Durán, M.A.; Revuelto, J.; López-Moreno, J.I. AVHRR warm-season cloud climatologies under various synoptic regimes across the Iberian Peninsula and the Balearic Islands. *Int. J. Climatol.* **2015**, *35*, 1984–2022. [CrossRef]
75. Schellenberger, T.; Ventura, B.; Zebisch, M.; Notarnicola, C. Wet Snow Cover Mapping Algorithm Based on Multitemporal COSMO-SkyMed X-Band SAR Images. *IEEE J. Sel. Top. Appl. Earth. Obs. Remote Sens.* **2012**, *5*, 1045–1053. [CrossRef]
76. Karam, M.; Amar, F.; Fung, A.; Mougin, E.; Lopes, A.; Le Vine, D.M.; Beaudoin, A. A microwave polarimetric scattering model for forest canopies based on vector radiative transfer theory. *Remote Sens. Environ.* **1995**, *53*, 16–30. [CrossRef]
77. Alonso-González, E.; Revuelto, J.; Fassnacht, S.R.; Ignacio López-Moreno, J. Combined influence of maximum accumulation and melt rates on the duration of the seasonal snowpack over temperate mountains. *J. Hydrol.* **2022**, *608*, 127574. [CrossRef]
78. Musselman, K.N.; Addor, N.; Vano, J.A.; Molotch, N.P. Winter melt trends portend widespread declines in snow water resources. *Nat. Clim. Chang.* **2021**, *2021*, 418–424. [CrossRef]
79. Wu, X.; Che, T.; Li, X.; Wang, N.; Yang, X. Slower snowmelt in spring along with climate warming across the Northern Hemisphere. *Geophys. Res. Lett.* **2018**, *45*, 12331–12339. [CrossRef]
80. Yang, Y.; You, Q.; Smith, T.; Kelly, R.; Kang, S. Spatiotemporal dipole variations of spring snowmelt over Eurasia. *Atmos. Res.* **2023**, *295*, 107042. [CrossRef]
81. Räisänen, J. Warmer climate: Less or more snow? *Clim. Dyn.* **2007**, *30*, 307–319. [CrossRef]
82. López-Moreno, J.I.; Gascoin, S.; Herrero, J.; Sproles, E.A.; Pons, M.; Alonso-González, E.; Hanich, L.; Boudhar, A.; Musselman, K.N.; Molotch, N.P.; et al. Different sensitivities of snowpacks to warming in Mediterranean climate mountain areas. *Environ. Res. Lett.* **2017**, *12*, 074006. [CrossRef]
83. Fassnacht, S.R.; Patterson, G.G.; Venable, N.B.H.; Cherry, M.L.; Pfohl, A.K.D.; Sanow, J.E.; Tedesche, M.E. How do we define climate change? Considering the temporal resolution of niveo-meteorological data. *Hydrology* **2020**, *7*, 38. [CrossRef]
84. Musselman, K.N.; Clark, M.P.; Liu, C.; Ikeda, K.; Rasmussen, R. Slower snowmelt in a warmer world. *Nat. Clim. Chang.* **2017**, *7*, 214–219. [CrossRef]
85. Verzano, K.; Menzel, L. Snow conditions in mountains and climate change—A global view. *IAHS-AISH Publ.* **2009**, 147–154. Available online: https://www.cabdirect.org/cabdirect/abstract/20093172872 (accessed on 23 March 2024).
86. Ishida, K.; Ohara, N.; Ercan, A.; Jang, S.; Trinh, T.; Kavvas, M.; Carr, K.; Anderson, M.L. Impacts of climate change on snow accumulation and melting processes over mountainous regions in Northern California during the 21st century. *Sci. Total Environ.* **2019**, *685*, 104–115. [CrossRef]
87. Nagler, T.; Rott, H.; Malcher, P.; Muller, F. Assimilation of meteorological and remote sensing data for snowmelt runoff forecasting. *Remote Sens. Environ.* **2008**, *112*, 1408–1420. [CrossRef]
88. Shi, J.; Dozier, J. Inferring snow wetness using C-band data from SIR-C's polarimetric synthetic aperture radar. *IEEE Trans. Geosci. Remote Sens.* **1995**, *33*, 905–914. [CrossRef]
89. Mätzler, C. Applications of the interaction of microwaves with the natural snow cover. *Remote Sens. Rev.* **1987**, *2*, 259–387. [CrossRef]
90. Ulaby, F.T.; Stiles, W.H.; Abdelrazik, M. Snow cover Influence on Backscattering from Terrain. *IEEE Trans. Geosci. Remote Sens.* **1984**, *22*, 126–133. [CrossRef]

91. Löw, A.; Ludwig, R.; Mauser, W. Land use dependent snow cover retrieval using multitemporal, multisensoral SAR images to drive operational flood forecasting models. In Proceedings of the EARSeL-LISSIG-Workshop on Observing our Cryosphere from Space, Bern, Switzerland, 11–14 March 2002.
92. Nagler, T.; Rott, H.; Ossowska, J.; Schwaizer, G.; Small, D.; Malnes, E.; Pinnock, S. Snow cover monitoring by synergistic use of Sentinel-3 Slstr and Sentinel-L Sar data. In Proceedings of the IEEE International Geoscience and Remote Sensing Symposium, Valencia, Spain, 22–27 July 2018. [CrossRef]
93. Dumont, M.; Gascoin, S. Optical Remote Sensing of Snow Cover. In *Book Land Surface Remote Sensing in Continental Hydrology*, 1st ed.; Baghdadi, N.A., Zibri, M., Eds.; ISTE Press—Elsevier: London, UK, 2016; pp. 115–137. [CrossRef]
94. Hall, D.K.; Riggs, G.A.; Salomonson, V.V. Development of methods for mapping global snow cover using moderate resolution imaging spectroradiometer data. *Remote Sens. Environ.* **1995**, *54*, 127–140. [CrossRef]
95. Hall, D.K.; Riggs, G.A.; Salomonson, V.V.; DiGirolamo, N.E.; Bayr, K.J. MODIS snow-cover products. *Remote Sens. Environ.* **2002**, *83*, 181–194. [CrossRef]
96. Vikhamar, D.; Solberg, R. Subpixel mapping of snow cover in forests by optical remote sensing. *Remote Sens. Environ.* **2003**, *84*, 69–82. [CrossRef]
97. Macander, M.J.; Swingley, C.S.; Joly, K.; Raynolds, M.K. Landsat-based snow persistence map for northwest Alaska. *Remote Sens. Environ.* **2015**, *163*, 23–31. [CrossRef]
98. Heinilä, K.; Salminen, M.; Pulliainen, J.; Cohen, J.; Metsämäki, S.; Pellikka, P. The effect of boreal forest canopy to reflectance of snow covered terrain based on airborne imaging spectrometer observations. *Int. J. Appl. Earth Obs. Geoinf.* **2014**, *27*, 31–41. [CrossRef]
99. Koskinen, J.; Pulliainen, J.; Hallikainen, M. The use of ERS-1 SAR data in snow melt monitoring. *IEEE Trans. Geosci. Remote* **1997**, *35*, 601–610. [CrossRef]
100. Magagi, R.; Bernier, M. Optimal conditions for wet snow detection using RADARSAT-SAT data. *Remote Sens. Environ.* **2003**, *84*, 221–233. [CrossRef]
101. Cohen, J.; Lemmetyinen, J.; Pulliainen, J.; Heinila, K.; Montomoli, F.; Seppanen, J.; Hallikainen, M.T. The effect of Boreal Forest Canopy in Satellite Snow Mapping—A Multisensor Analysis. *IEEE Trans. Geosci. Remote* **2015**, *53*, 6593–6607. [CrossRef]
102. Baghdadi, N.; Gauthier, Y.; Bernier, M.; Fortin, J.P. Potential and limitations of RADARSAT SAR data for wet snow monitoring. *IEEE Trans. Geosci. Remote* **2000**, *38*, 316–320. [CrossRef]